ELSEVIER

Materials Science and Engineering B47 (1997) 119–126

MATERIALS SCIENCE & ENGINEERING B

An optical study of the athermal photo-amorphization of $As_{50}Se_{50}$ thin films

C. Corrales [a,*], J.B. Ramírez-Malo [b], E. Márquez [b], R. Jiménez-Garay [b]

[a] *Departamento de Ingeniería de Sistemas y Automática, Facultad de Ciencias Náuticas, Universidad de Cádiz, Ap. 40, 11510-Puerto Real (Cádiz), Spain*

[b] *Departamento de Física de la Materia Condensada, Facultad de Ciencias, Universidad de Cádiz, Ap. 40, 11510-Puerto Real (Cádiz), Spain*

Received 19 September 1996

Abstract

In this paper we report on a study of a novel photo-induced structural effect in amorphous chalcogenide materials, namely the reversible and athermal light-induced vitrification of $As_{50}Se_{50}$ thin films. The first optical analysis of this phenomenon presented here was done by applying two different non-destructive methods. One is based on the optical transmittances of the interference maxima and minima at normal incidence, and takes into account the lack of thickness uniformity of the chalcogenide glass films. The other optical method, however, is based only on the shift undergone by the wavelengths of the interference extrema when the incidence changes from normal to oblique. On the other hand, the refractive-index behaviour of the as-evaporated, crystallized and photo-vitrified films under study is analyzed within the oscillator framework proposed by Wemple and DiDomenico. Finally, the absorption edge is described using the non-direct transition model proposed by Tauc. © 1997 Elsevier Science S.A.

Keywords: $As_{50}Se_{50}$ thin films; Optical study; Athermal photo-amorphization

1. Introduction

Because the information storage density in optical media can be up to two magnitude orders better than in magnetic discs, there has been extensive research into materials capable of optical recording. Chalcogenide films have potential in this area and have been investigated as optical recording media for mass–memory applications such as data discs for video recording or computer information storage [1]. In these applications, among the basic mechanisms used to record information is the photo-induced amorphization of a crystalline film [2]. In this phase-transition mechanism, the optical constants of the amorphous and crystalline materials are sufficiently different that discrimination between the exposed and unexposed regions of the film can be achieved by monitoring reflectance.

In this work, we report the effect of photo-amorphization of $As_{50}Se_{50}$ semiconducting thin films, previously crystallized by annealing [3]. Unlike crystallization, photo-amorphization is an athermal process because the intensity of the actinic light is not able to cause an increase in temperature giving way to a phase-transition phenomenon. Furthermore, it must be emphasized that the crystallization through annealing and amorphization by light processes are reversible. We have carried out the annealing-illumination cycle three times, and using the methods presented here, we have been able to determine the changes in the optical constants and in the morphology of the films, for the first two cycles. We must also note that, with the characteristics mentioned, this phenomenon only takes place in films of the $As_{50}Se_{50}$ glassy composition. For instance, our attempts to crystallize amorphous $As_{30}Se_{70}$, $As_{40}Se_{60}$ and $As_{60}Se_{40}$ films, by annealing them for 72 h as a prelude to investigating photo-vitrification, have failed.

These amorphization and crystallization processes in chalcogenide films can be accompanied by morphological, such as photovolumetric changes [4,5], which must be taken into account in order to determine the optical constants of the films. With this aim in view, a non-destructive method, based only on the optical transmission spectrum at normal incidence, has been applied to

* Corresponding author.

PII S0921-5107(97)00030-5

simultaneously calculate refractive index, average thickness and a parameter indicating the degree of non-uniformity of the film thickness [6,7]. When the lack of uniformity of the film thickness is very strong, this method may be unable to correctly determine the average thickness and refractive index, and a second procedure, based also on the optical interference spectrum at oblique incidence, is used to calculate them [8,9]. In both cases, the absorption coefficients and optical band gap are also determined.

2. Experimental details

The thin-film samples were prepared by vacuum evaporation of powdered melt-quenched material onto clean glass substrates (BDH microscope slides). The thermal evaporation process was carried out in a coating system (Edwards, model E306A) at a pressure of $\approx 5 \times 10^{-7}$ Torr, from a suitable quartz crucible. The temperature rise of the substrate due to radiant heating from the crucible was negligible. During evaporation, the substrates were rotated (≈ 45 rpm) in order to obtain an enhanced degree of film thickness uniformity and the deposition rate was ≈ 1 nm s^{-1}, this quantity having been continuously measured by a quartz-crystal monitor (Edwards, model FTM-5).

The film thicknesses were in the 700–1200 nm range. The samples were annealed at 150°C ($T_g = 164$°C) for periods of, typically, 72 h in a $\approx 10^{-3}$ Torr vacuum. Illumination of the glass films was carried out using a 500 W high-pressure mercury lamp (Oriel, model 66032), through an IR-cut filter, providing broadband white light (with a very high UV output).

The optical transmission spectra were obtained by a double-beam, ratio recording UV/VIS/NIR computer-controlled spectrophotometer (Perkin-Elmer, model Lambda-19) and are shown, together with the XRD patterns (obtained using a Philips, model PW-1830 X-ray diffractometer, with Cu Kα radiation), in Figs. 1 and 2.

3. Calculation procedures

3.1. Normal incidence

The transmission $T_{\Delta d}$ in the transparent region at a specific wavelength λ, for the case of non-uniform thickness, can be obtained by [7,10]

$$T_{\Delta d} = \frac{1}{\varphi_2 - \varphi_1} \int_{\varphi_1}^{\varphi_2} \frac{A}{B - C\cos\varphi + D}\, d\varphi \qquad (1)$$

where $A = 16n^2 s$, $B = (n+1)^3(n+s^2)$, $C = 2(n^2-1)(n^2-s^2)$, $D = (n-1)^3(n-s^2)$, $\varphi = 4\pi nd/\lambda$ with $\varphi_1 = 4\pi n(\bar{d} - \Delta d)/\lambda$ and $\varphi_2 = 4\pi n(\bar{d} + \Delta d)/\lambda$. It is assumed that the thickness varies linearly over the area illuminated by the spectrophotometer, so that the thickness is: $d = \bar{d} \pm \Delta d$. Δd refers to the actual variation in thickness from the average thickness $\bar{d}$ and s is the refractive index of the substrate. This refractive index was previously determined over the whole spectral range, from the transmission spectrum of the substrate with no material deposited. The expressions for the envelopes around the interference maxima and minima of the optical transmission spectrum are the following [7]:

$$T_{Md,md} = \frac{2a}{\Delta\varphi(1-b^2)^{1/2}} \tan^{-1}\left[\frac{1 \pm b}{(1-b^2)^{1/2}} \tan\left(\frac{\Delta\varphi}{2}\right)\right] \qquad (2)$$

where + in the $\pm$ refers to $T_{Md}(\lambda)$ and − to $T_{md}(\lambda)$; $a = A/(B+D)$, $b = C/(B+D)$ and $\Delta\varphi = \varphi_2 - \varphi_1$. The validity range of Eq. (2) is: $0 < \Delta d < \lambda/4n$. In addition, the two expressions included in Eq. (2) are two independent transcendental equations with only two unknown parameters, n and Δd. They have been successfully solved for the experimental values using a standard computer method (Newton–Raphson iteration).

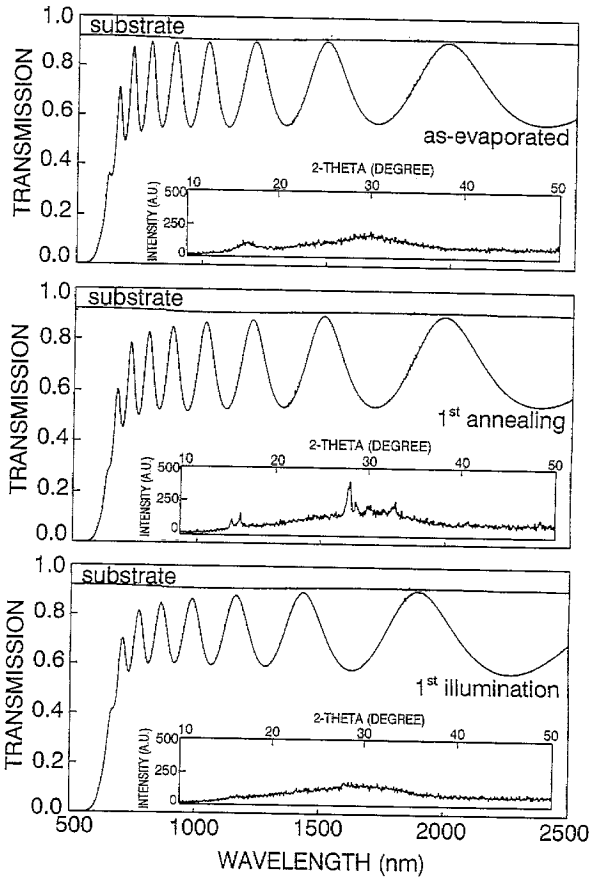

Fig. 1. Typical optical transmission spectra and X-ray diffraction patterns (Cu Kα radiation) for the as-deposited, crystallized and photo-amorphized $As_{50}Se_{50}$ thin film, respectively.

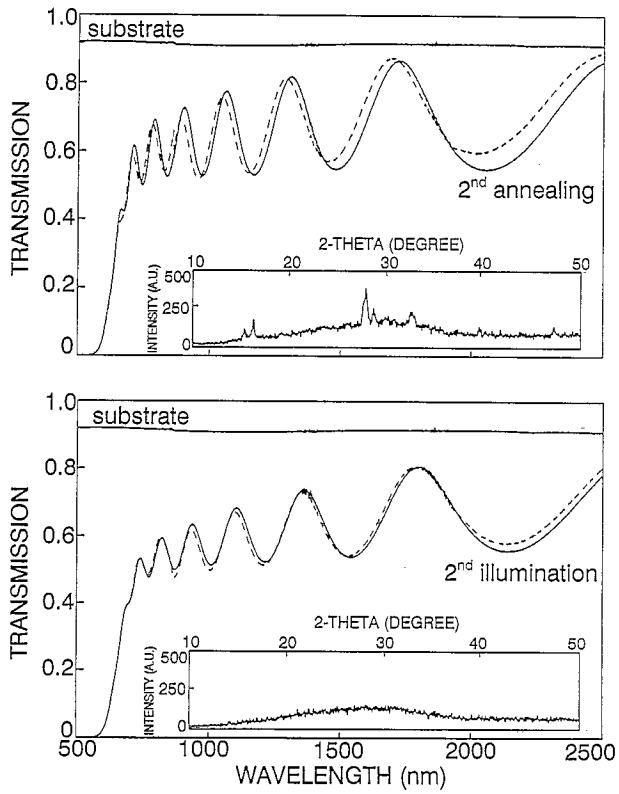

Fig. 2. Optical transmission spectra and X-ray diffraction patterns for the crystallized and photo-vitrified $As_{50}Se_{50}$ thin film, respectively, corresponding to a second cycle.

Moreover, in the region of weak and medium absorption ($\alpha > 0$), the integration Eq. (1) should be done over both the film thickness variation and absorbance. This is prohibitively difficult analytically and an approximation would be to consider x to have an average value over the integration range with respect to Δd. This is an excellent approximation provided $\Delta d \ll \bar{d}$. The constants a and b are now redefined as follows: $a_x = Ax/(B + Dx^2)$, $b_x = Cx/(B + Dx^2)$, being $x = \exp(-\alpha\bar{d})$. The equations for the two envelopes now become

$$T_{Mx,mx} = \frac{2a_x}{\Delta\varphi(1-b_x^2)^{1/2}} \tan^{-1}\left[\frac{1 \pm b_x}{(1-b_x^2)^{1/2}} \tan\left(\frac{\Delta\varphi}{2}\right)\right] \quad (3)$$

where again + in the $\pm$ refers to $T_{Mx}(\lambda)$ and − to $T_{mx}(\lambda)$. These expressions are again two independent transcendental equations with two unknown parameters, n and x, since Δd is known from solving Eq. (2) in the transparent region. Eq. (3) again has one solution only for n and x in the range: $0 < x \leq 1$. In addition, these last n-values can be used for determining the average thickness from the basic equation for the interference fringes

$$2n\bar{d} = m\lambda \quad (4)$$

where m has integer values for the maxima and half-integer values for the minima. Furthermore, we shall consider that n is larger than the substrate refractive index.

Next, the spectral dependence of the refractive index is fitted to the Wemple–DiDomenico dispersion relationship, that is, the single-oscillator model [11]

$$\varepsilon_1(E) = n^2(E) = 1 + \frac{E_0 E_d}{E_0^2 - E^2} \quad (5)$$

where E_0 is the single-oscillator energy (typically near the main peak of the $\varepsilon_2(E)$-spectrum) and E_d is the dispersion energy. The latter parameter obeys the simple empirical relationship, $E_d = \beta N_c Z_a N_e$, where β is a constant, N_c is the number of nearest neighbour cations to the anion, Z_a is the formal chemical valency of the anion and N_e is the effective number of valence electrons per anion.

The applicability of this first procedure for determining the optical dispersion and average thickness is limited by the aforementioned condition, $0 < \Delta d < \lambda/4n$. In this work, we have however only been able to apply it to the optical characterization of films that were as-deposited, and later crystallized and photo-vitrified only once.

On the other hand, in the strong absorption region, where the interference fringes disappear, the absorbance values x are determined from [7]

$$x \approx \frac{(n+1)^3(n+s^2)}{16n^2 s} T \quad (6)$$

Once x and $\bar{d}$ are known, the absorption coefficient α is determined directly, using the expression $\alpha = -(1/\bar{d}) \ln x$. Next, the absorption coefficient of amorphous semiconductors in the high-absorption region ($\alpha \gtrsim 10^4$ cm^{-1}), assuming parabolic band edges and energy-independent matrix elements for interband transitions, is given according to the non-direct transition model proposed by Tauc [12], by the following equation

$$\alpha(h\nu) = K_1 \frac{(h\nu - E_g^{opt})^2}{h\nu} \quad (7)$$

where $h\nu$, E_g^{opt} and K_1, denote the photon energy, optical energy gap and an energy-independent constant, respectively. The optical gap E_g^{opt} is therefore obtained formally as the intercept of the plot of $(\alpha h\nu)^{1/2}$ against $h\nu$.

It is worth noting that the above-described procedures has been successfully used in the optical characterization of glassy films of As–S, As–Se and Ge–Se alloys [13–15], and also in the optical study of the Ag-photodissolution phenomenon in As–S films [16].

Table 1
Values of the average thickness $\bar{d}$, thickness variation Δd, refractive index extrapolated to $E=0$ and at $\lambda=1000$ nm, $n(0)$ and $n(1000)$, dispersion parameters E_0 and E_d (single-oscillator analysis) and optical band gap E_g^{opt} (Tauc's extrapolation) for the thin films under study

Sample state	$\bar{d}$ (nm)	Δd (nm)	$n(0)$	$n(1000)$	E_0 (eV)	E_d (eV)	E_g^{opt} (eV)
As-deposited	1123 ± 11	17	2.617	2.734	3.98	23.29	1.86
First annealing	1062 ± 19	27	2.762	2.902	3.79	25.11	1.82
First illumination	1108 ± 31	35	2.521	2.668	3.52	18.85	1.76
Second annealing	930 ± 35	—	2.728	2.862	3.83	24.68	1.81
Second illumination	1030 ± 39	—	2.568	2.703	3.68	20.59	1.73

3.2. Oblique incidence

This new, useful second method has been applied for characterizing films which were crystallized, and then vitrified, in the second annealing and illumination cycle. The analysis that follows is based on the assumption that a mathematical expression for dispersion $n(\lambda)$ exists. It is also assumed that n is isotropic. From the theory of normal dispersion [17], as well as from practical experience, it follows that the spectral dependence of the refractive index can also be represented very accurately by three constants, x, a and b in the region $k^2 \ll n^2$:

$$n^2 = \frac{a}{\lambda^x} + b \tag{8}$$

Furthermore, for normal incidence on a film with thickness d, the wavelengths of the transmission extrema are given by Eq. (4), as $2n_0 d = m\lambda_0$.

The problem is thus reduced to determining five constants, m, d, x, a and b, from the transmission spectrum. Only m and x, apart from the product $n_0 d$, can be determined solely from Eqs. (4) and (8), and another experimental equation must be found. This can be done by obtaining a second transmission spectrum at an angle of incidence $i > 0$ (see Fig. 2). The equation for the interference extrema now becomes [18]

$$2n_i d \cos r = m\lambda_i \tag{9}$$

where r is the angle of refraction in the film. The five constants can now be found from Eqs. (4), (8) and (9) in various ways, provided that at least three extrema are available.

In Fig. 2 the solid spectra show the transmission spectra for normal incidence in the transparent and absorption regions corresponding to the second cycle. The broken spectra are the spectra at an incidence angle of 30°, and the whole spectra shift towards the shorter-wavelength region according to Eq. (9).

3.2.1. Determining n from the order numbers m

We now consider m not to be a discrete-order number but a continuous mathematical variable. The spectrum for normal incidence can be shifted towards shorter wavelengths by increasing each order number by an amount Δm, where Δm can be different for each m. The shifting due to oblique incidence according to Eq. (9) can thus be written in terms of normal incidence as

$$2n_i d = (m + \Delta m)\lambda_i \tag{10}$$

From Eqs. (9) and (10), and Snell's law, it follows that

$$\cos r = \frac{m}{m + \Delta m} \tag{11}$$

$$n_i = \frac{\sin i}{\sin r} \tag{12}$$

Considering two adjacent extrema of the normal-incidence spectrum at wavelengths λ_{01} and λ_{02}, it follows from Eq. (4) that

$$m_1 = \frac{n_{01}\lambda_{02}}{2(n_{02}\lambda_{01} - n_{01}\lambda_{02})}$$

The quantity M is now defined as

$$M = \frac{\lambda_{02}}{2(\lambda_{01} - \lambda_{02})} \tag{13}$$

where $M \geq m_1$. The equality $M = m_1$ is true only in the absence of dispersion. The effect of dispersion on M can be approximated by a mathematical function of the form

$$M = \frac{C}{\lambda_0}\left(1 + \frac{D}{\lambda_0^y}\right) \tag{14}$$

The first term in Eq. (14) reflects the $1/\lambda$ relation between m and λ according to Eq. (8), while the term in parentheses approximates the effect of dispersion. The value of m at each extremum is now approximately given by $m \approx C/\lambda_0$. Eq. (14) can be written in the form of an equation for a straight line:

$$M\lambda_0 = \frac{DC}{\lambda_0^y} + C \tag{15}$$

The value of y can be determined by iterating y and performing a linear regression of Eq. (15). The value of y is chosen to give a good fit to Eq. (15), and yields values of m, according to the approximation $m \approx C/\lambda_0$, that differ by 1/2, and also yield correct approximate integer or half-integer values for each corresponding

extremum: from the approximate values of m, exact-order numbers can now be assigned to each extremum.

Substitution of Eq. (8) into Eq. (4), for normal incidence, yields

$$m^2\lambda_0^2 = \frac{A}{\lambda_0^x} + B \tag{16}$$

where $A = 4ad^2$ and $B = 4bd^2$.

Since the order numbers are known, the value of x can be determined by iteration and performing a linear regression of Eq. (16). The value of x that gives the best fit to experimental values is chosen, and the regression also yields the values of A and B.

Substituting Eq. (4) into Eq. (10), using Eq. (16), and solving for Δm yields

$$\Delta m = \left[m^2 \frac{\lambda_0^2}{\lambda_i^2} + \frac{A}{\lambda_i^2}\left(\frac{1}{\lambda_i^x} - \frac{1}{\lambda_0^x}\right)\right]^{1/2} - m \tag{17}$$

The value of n_i at each value of λ_i can now be calculated using Eqs. (17), (11) and (12).

The value of d can be determined by using the fact that m increases by 1/2 for each successive extremum described by Eq. (10). If m_1 is the order number of the first extremum considered at the long-wavelength end, Eq. (10) can be written for the successive extrema as

$$\frac{j}{2} + \Delta m = 2d\frac{n_i}{\lambda_i} - m_1 \tag{18}$$

where $j = 0, 1, 2, 3\ldots$. A straight line through $-m_1$ and the other points has a slope $2d$, and the value of d can be obtained from this slope. Once d is known, a and b can be calculated from Eq. (16), which completes the calculation of the required five constants.

3.2.2. Determining n from the dispersion equation

An alternative way of calculating n independently from m will now be considered. From Eqs. (9) and (4) for normal incidence, it follows that

$$n_i \cos r = n_0 \frac{\lambda_i}{\lambda_0} \tag{19}$$

In the non-dispersive case Eq. (19) becomes

$$\cos r = \frac{\lambda_i}{\lambda_0} \tag{20}$$

and n can be calculated directly from Eq. (12).

Eq. (19) can be written as

$$n_i^2(1 - \sin^2 r) = n_0^2 \frac{\lambda_i^2}{\lambda_0^2}$$

Substituting Eq. (12) into the above equation yields

$$n_i^2 - n_0^2 \frac{\lambda_i^2}{\lambda_0^2} = \sin^2 i \tag{21}$$

On the other hand, from Eq. (4), by expanding n_i^2 in a Taylor series around n_0, it follows that

$$n_i^2 = n_0^2 + \frac{ax}{\lambda_0^{x+1}}(\lambda_0 - \lambda_i) \tag{22}$$

Substituting Eq. (22) into Eq. (21) yields

$$n_0^2 = N^2 - \frac{ax}{\lambda_0^{x-1}(\lambda_0 + \lambda_i)} \tag{23}$$

where

$$N^2 = \frac{\lambda_0^2 \sin^2 i}{\lambda_0^2 - \lambda_i^2} \tag{24}$$

Eqs. (4) and (23) show that N^2 can also be represented by a function of the form

$$N^2 = \frac{E}{\lambda^x} + b \tag{25}$$

From Eqs. (4), (25) and (23) it follows that

$$\frac{E}{a} = \frac{(1+x)\lambda_0 + \lambda_i}{\lambda_0 + \lambda_i} \approx 1 + \frac{x}{2} \tag{26}$$

x can thus be determined by calculating N^2 for each extremum and iterating x to give a good fit to Eq. (25). This regression also yields the values of E and b. The value of a can be determined from Eq. (26); hence $n(\lambda)$ is thus determined.

To determine m and d, an equation similar to Eq. (18) can be written as

$$\frac{j}{2} = 2d\frac{n_0}{\lambda_0} - m_1 \tag{27}$$

Extrapolation of a straight line through these points will indicate the order number of the first extremum, m_1. A straight line through $-m_1$ and the points again has a slope $2d$ from which d can be determined. This completes the calculation of the required five constants.

Finally, by simply substituting the average thicknesses and the previously derived order numbers in Eq. (4), we can calculate the refractive index for the wavelengths of each interference extremum at normal incidence, encompassing both methods at oblique incidence [9]. On the other hand, although these refractive indices have been calculated from a predetermined dispersion relationship, Eq. (8), they can be refitted to the above-mentioned Wemple–DiDomenico relationship, Eq. (5), enabling us to determine the dispersion parameters E_0 and E_d, which correspond to the second crystallization and subsequent photovitrification. The absorption coefficients and Tauc gap are determined as already described.

The optical transmission spectra at normal and oblique incidence were obtained by placing the films on an accurate goniometer set up inside the spectrophotometer. At oblique incidence the transmission spectrum shifts, within the interference region, towards shorter wavelengths than at normal incidence. The incidence angle chosen was 30°: a smaller angle produces a smaller shift of the interference extrema of the optical

transmission spectrum at oblique incidence, thus making the calculations, based on the difference $\lambda_0 - \lambda_i$, less accurate. A larger incidence angle is not advisable either, as the polarization effect may influence the optical transmittance values, thus deforming the spectra [19].

4. Results and discussion

One aspect of the diffraction results on chalcogenide materials has been ascribed to the influence of medium-range order, and this is the so-called first sharp diffraction peak (FSDP) or prepeak in the structure factor [20]. This peak almost invariably occurs at a value of the modulus of the scattering vector of ≈ 1 Å^{-1} in amorphous chalcogenides. The $As_{50}Se_{50}$ thin-film samples could be crystallized by annealing at ≈ 140°C for periods up to 72 h, and show a very significant diffraction peak for $2\theta = 27.9°$, and less pronounced ones for $2\theta = 15.4°$, 16.4°, 28.6°, 32.4°, 32.8° and 48.3°. By comparing the peak positions in the X-ray diffraction patterns to powder-diffraction data for As–Se binary crystals taken from Ref. [21], we can unambiguously identify the crystalline phase of the film as c-As_4Se_4 (the corresponding crystal system is monoclinic). However, it must be noted that the relative intensities of the peaks show small differences in relation to those tabulated in Ref. [21], hinting at possible preferential orientations in the crystallized film with respect to the substrate plane [22]. Also worth nothing is the virtual absence of FSDP at $2\theta \approx 17°$, characteristic of the amorphous phase corresponding to the as-deposited film, in the crystallized material.

Recent studies [23] have shown that the crystallization process depends clearly on the thickness of the $As_{50}Se_{50}$ films. Thus, in very thin (0.2–0.5 μm) films, crystallization is incomplete, and in thick (3–5 μm), the XRD patterns show more crystallization peaks than in films of medium (1–2 μm) thickness, the most dominant peak for thick films is also the one at $2\theta = 27.9°$, which shows a lower relative intensity. In this work, the optically-characterized films have a thickness of ≈ 1 μm, in order to observe more clearly the dominant peak, and also to ensure that the light is homogeneously absorbed by the material.

When the film is illuminated, its crystalline nature disappears, giving way to photo-amorphization. Elliott and Kolobov [3] use a quartz-tungsten halogen lamp as a light source, and observed that the XRD pattern of the photovitrified film is similar to that of the as-deposited film. However, in this work, in which a mercury lamp was used, FSDP practically disappeared in the first vitrification, and was completely absent in the second [4]. This fact may be due to the difference between the spectral irradiances of the two light sources, since the mercury lamp has a higher UV content than the quartz-tungsten halogen lamp, and so part of the photons will have higher energy and will obviously produce a larger degree of disorder in the material.

When the as-evaporated film is annealed, an irreversible shift of the optical transmission spectrum towards longer wavelengths is observed in the interference-free region (thermal-darkening). The subsequent illumination of the film induces again a shift of the optical transmission spectrum towards longer wavelengths, but it is reversible photo-darkening. A second annealing produces another reversible shift, this time towards shorter wavelengths (thermal-bleaching). Lastly, another illumination produces another photo-darkening. The athermal vitrification process can therefore be considered, from an optical point of view, as a clear photo-darkening phenomenon, widely studied in other amorphous chalcogenide compositions [13,24,25].

The values of parameter Δd, representing the degree of uniformity in the film thickness, show that it increases with exposure to the different treatments. The films submitted to a second annealing and illumination cycle show a high degree of morphological alteration. The optical transmission spectra are so deformed that the method based only on measuring optical transmittance at normal incidence ceases to be applicable. For this reason, the second method at oblique incidence was used to optically characterize these films.. The decrease in the average thickness of the films, due to annealing, is a clear sign of a thermal densification process, whereas the increase which takes place with illumination constitutes obviously a photoinduced volume expansion.

The refractive index increases with annealing and decreases with illumination, under the initial value (Fig. 3); the shifts of the optical absorption edge and the variations in the Tauc gap (Fig. 4) are similar to those usually observed in the photo-darkening phenomenon. The trend of the dispersion energy E_0 is the same as the optical gap, thus verifying the relationship $E_0 \approx 2E_g^{opt}$ found by Tanaka [26] and confirmed for other glassy systems [13–16]. The dispersion parameter E_d obeys the proportional relationship $E_d \propto N_c$, where N_c is, in this particular case, the As effective coordination number. The variation shown by E_d implies that, as deduced from the XRD patterns, important structural changes take place during the athermal photo-amorphization process in $As_{50}Se_{50}$ films. Crystallization is related to a higher value for E_d, in comparison to the initial value (as-deposited film), and amorphization to a value lower one.

Lastly, there are two possible models for explaining the mechanism of photo-induced vitrification [23,27]. One is based on the breaking of covalent bonds, within the As_4Se_4 molecules which make up the crystalline

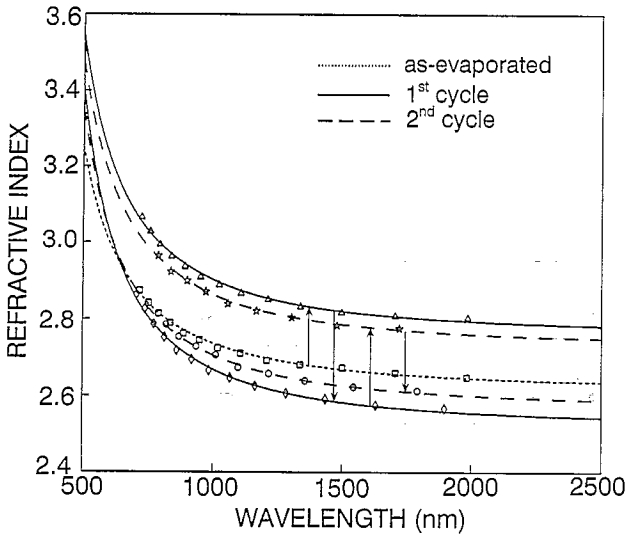

Fig. 3. Refractive index as a function of wavelength for the as-deposited $As_{50}Se_{50}$ thin film on a glass substrate and after two annealing-illumination cycles.

structure (intramolecular bond-breaking); an amorphous cross-linked network would be the outcome. The other model takes into consideration the fact that changes take place in the relative orientation and spatial distribution of the As_4Se_4 molecules, due to photo-induced intermolecular bond-breaking, resulting in a translationally and orientationally disordered amorphous phase in which the integrity of the As_4Se_4 molecules is preserved.

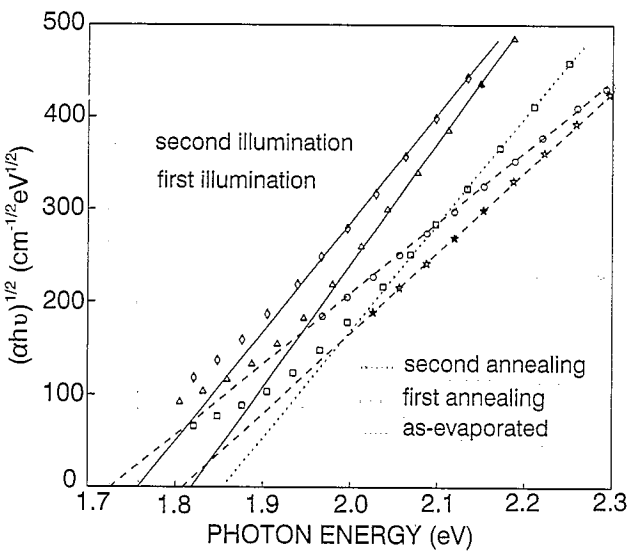

Fig. 4. Determination of the optical band gap in terms of the Tauc law corresponding to the phenomenon of athermal light-induced vitrification of $As_{50}Se_{50}$ film.

5. Conclusions

For the first time, the athermal photo-vitrification phenomenon has been optically characterized, in two annealing and illumination cycles. This phenomenon takes place only in $As_{50}Se_{50}$ films. The morphological changes undergone by the films, because of the successive thermal and optical treatments, made it necessary to use two different optical characterization methods. One is based solely on the optical transmission spectrum at normal incidence, whereas the other is based only on the wavelengths of the interference extrema at normal and oblique incidence. The optical constants and Tauc gaps, thus determined, lead us to the conclusion that the photo-induced phenomenon under study is accompanied by a clear reversible photo-darkening process.

Acknowledgements

The authors would like to acknowledge some very useful discussions with A.V. Kolobov.

References

[1] C.M.J. Van Uijen, Optical mass data storage, SPIE 529 (1985) 2.
[2] M. Uchida, K. Yoshioka, K. Inoue, T. Akiyama, S. Furukawa, K. Kotera, S. Nakamura, Proc. Soc. Photo-Opt. Instrum. Eng. SPIE 1078 (1989) 27.
[3] S.R. Elliott, A.V. Kolobov, Athermal light-induced vitrification of $As_{50}Se_{50}$ films, J. Non-Cryst. Solids 128 (1991) 216.
[4] E. Marquez, C. Corrales, J.B. Ramirez-Malo, J. Reyes, J. Fernandez-Peña, P. Villares, R. Jimenez-Garay, On the reversible and athermal photo-vitrification phenomenon of $As_{50}Se_{50}$ chalcogenide thin films, Mater. Lett. 20 (1994) 183.
[5] K. Tanaka, Photo-induced structural changes in chalcogenide glasses, Rev. Solid State Sci. 4 (1990) 641.
[6] R. Swanepoel, Determination of the thickness and optical constants of amorphous silicon, J. Phys. E 16 (1983) 1214.
[7] R. Swanepoel, Determination of the surface roughness and optical constants of inhomogeneous amorphous silicon films, J. Phys. E 17 (1984) 896.
[8] R. Swanepoel, Determining refractive index and thickness of thin films from wavelength measurements only, J. Opt. Soc. Am. A 2 (1985) 1339.
[9] C. Corrales, J.B. Ramirez-Malo, J. Fernandez-Peña, P. Villares, R. Swanepoel, E. Marquez, Determining the refractive index and average thickness of As–Se semiconducting glass films from wavelength measurements only, Appl. Opt. 34 (1995) 7907.
[10] C.J. Manifacier, J. Gasiot, J.P. Fillard, A simple method for the determination of the optical constants n, k and the thickness of weakly absorbing film, J. Phys. E 9 (1976) 1002.
[11] S.H. Wemple, Refractive-index behavior of amorphous semiconductors and glasses, Phys. Rev. B 7 (1973) 3767.
[12] J. Tauc, in: Proc. Int. Conf. Physics of Semiconductors, Cambridge, 1970, p. 159.
[13] C. Corrales, Optical properties and photoinduced effects in thin films of the As–Se glassy semiconducting system, PhD dissertation, Departamento de Estructura y Propiedades de los Materiales, Universidad de Cádiz, Cádiz, Spain, 1994.

[14] E. Marquez, J.B. Ramirez-Malo, P. Villares, R. Jimenez-Garay, R. Swanepoel, Optical characterization of wedge-shaped thin films of amorphous arsenic trisulphide based only on their shrunk transmission spectra, Thin Solid Films 254 (1995) 83.
[15] J. Reyes, E Marquez, J.B. Ramirez-Malo, C. Corrales, J. Fernandez-Peña, P. Villares, R. Jimenez-Garay, Optical constants of thermally-evaporated amorphous $GeSe_3$ thin films, J. Mater. Sci. 30 (1995) 4133.
[16] E. Marquez, J.B. Ramirez-Malo, J. Fernandez-Peña, R. Jimenez-Garay, P.J.S. Ewen, A.E. Owen, On the optical properties of wedge-shaped thin films of Ag-photodoped $As_{30}S_{70}$ glass, Opt. Mater. 2 (1993) 143.
[17] F.S. Crawford, Waves, McGraw-Hill, New York, 1968, p. 182.
[18] A. Nussbaum, R.A. Phillips, Contemporary Optics for Scientists and Engineers, Prentice Hall, Englewood Cliffs, NJ, 1976, p. 168.
[19] G.R. Fowles, Introduction to Modern Optics, Holt, Rinehart and Winston, New York, 1975, p. 44.
[20] S.C. Moss, D.L. Price, in: D. Adler, H. Fritzche, S.R. Ovshinsky (Eds.), Physics of Disordered Materials, Plenum Press, New York, 1985, p. 77.
[21] Powder Diffraction File, Inorganic Phases, JCPDS International Centre for Diffraction Data, 1988.
[22] A.V. Kolobov, V.A. Bershtein, S.R. Elliott, Athermal photoamorphization of $As_{50}Se_{50}$ films, J. Non-Cryst. Solids 150 (1992) 116.
[23] A.V. Kolobov, S.R. Elliott, Reversible photo-amorphization of a crystallized $As_{50}Se_{50}$ alloy, Philos. Mag. B 71 (1995) 1.
[24] G. Pfeiffer, M.A. Paesler, S.C. Agarwal, Reversible photodarkening of amorphous arsenic chalcogens, J. Non-Cryst. Solids 130 (1991) 111.
[25] I. Shimizu, H. Fritzsche, Thickness and refractive-index changes associated with photodarkening in evaporated As_2S_3 films, J. Appl. Phys. 47 (1976) 2969.
[26] K. Tanaka, Optical properties and photoinduced changes in amorphous As–S films, Thin Solid Films 66 (1980) 271.
[27] A.V. Kolobov, S.R. Elliott, Reversible photo-amorphization of crystalline films of $As_{50}Se_{50}$, J. Non-Cryst. Solids 189 (1995) 297.